Available online at www.sciencedirect.com

ScienceDirect

journal homepage: http://www.elsevier.com/locate/acme

Original Research Article

Microstructural evolution and development of mechanical properties of spark plasma sintered WC–Co cemented carbides for machine parts and engineering tools

D. Garbiec [a,*], P. Siwak [b]

[a] Metal Forming Institute, 14 Jana Pawla II Street, 61-139 Poznan, Poland
[b] Poznan University of Technology, 5 Marii Sklodowskiej–Curie Square, 60-965 Poznan, Poland

ARTICLE INFO

Article history:
Received 30 March 2018
Accepted 20 October 2018
Available online

Keywords:
Cemented carbides
Spark plasma sintering
Microstructure
Mechanical properties

ABSTRACT

WC–Co, WC–Co–Cr_3C_2 and WC–Co–TaC–NbC cemented carbides were spark plasma sintered and the microstructure and main mechanical properties of the obtained specimens were investigated. A series of WC–6Co cemented carbides was heated to the sintering temperature of 1400 °C at 200 and 400 °C/min at compacting pressures of 50 and 60 MPa. It was shown that the specimens spark plasma sintered at 400 °C/min and at 60 MPa possess the best mechanical properties. These parameters were applied for sintering WC–6Co cemented carbides with addition of grain growth inhibitors such as Cr_3C_2 and TaC–NbC. The influence of the grain growth inhibitors content was studied. The X-ray diffraction test results show that decarburization of the WC phase occurred and carbon deficient W_2C and η (Co_3W_3C, Co_6W_6C) phases were formed during spark plasma sintering, wherein an increase in compacting pressure from 50 to 60 MPa results in a diminution in the carbon diffusion processes. The mechanical properties of the cemented carbides were defined. The best ratio of hardness and fracture toughness was obtained for WC–6Co–1Cr_3C_2: hardness was 1808 ± 19 HV_{30} and fracture toughness was 10.17 ± 0.27 MPa $m^{1/2}$.

1. Introduction

Despite the fact that tungsten carbide–cobalt (WC–Co) hard materials cause allergies and contain probable human carcinogenic agents [1,2], they are still the most dominant tool materials in terms of industrial applications for machining, mining, cutting and drilling tools as well as wear resistance parts. WC–Co cemented carbides display a unique combination of mechanical properties such as high hardness,

* Corresponding author.
E-mail address: dariusz.garbiec@inop.poznan.pl (D. Garbiec).
https://doi.org/10.1016/j.acme.2018.10.004

excellent wear resistance, good toughness and strength than that of other hard materials [3–6]. Morphologically, they consist of the hard hexagonal WC ceramic phase embedded within a soft and tough Co binder phase. Increasing of the WC phase content in the sintered compacts leads to raising of the hardness and wear resistance and decrease of the fracture toughness [6]. Moreover, the presence of secondary phases synthesized in the sintered compacts as a result of decarburization of the WC phase, and carbon diffusion during sintering may reduce its mechanical properties [7].

It is well known at present time that industrial interests are focused on synthesis of WC–Co cemented carbides with high hardness and fracture toughness. These materials with a reduced grain size to a submicron meter or nanometer range can meet the growing demands of industry. Thus WC-based and other nanocrystalline materials have received a great deal of attention as advanced engineering materials with improved physical and mechanical properties [3–6,8]. As shown by Liu et al. [4], the hardness, strength and toughness of WC–Co cemented carbides improve greatly when the WC grain size is reduced to below 500 nm. However, the rapid growth of ultrafine WC grains occurs during heating even though the liquid phase is not formed. A variety of new sintering technologies are employed to diminish the effect of grain growth and to achieve an efficient WC–Co material densification [8,9]. The densification of WC–Co powder mixture has been accomplished by conventional sintering [10], hot pressing (HP) [11], hot isostatic pressing (HIP) [12], microwave sintering [9,13], high-frequency induction sintering [14,15], pulse plasma compaction (PPC) [16] and spark plasma sintering (SPS) [17,18]. The SPS technique has a well-known advantages owing to its such as rapid heating and cooling rates, short holding time and small compacting pressure changes. For this reason, this technology has attracted increasingly more attention in the investigations of nanocrystalline and ultrafine WC–Co cemented carbides. As shown by [4,8,18], grain growth during SPS can be effectively inhibited. Modifying the microstructure of WC–Co cemented carbides with grain growth inhibitors such as Cr_3C_2 [19], TaC [20,21], TiC [21], VC [20] and NbC [22] can efficiently inhibit WC grain growth and allow one to increase both the hardness and fracture toughness.

The purpose of this paper, which is a continuation of the paper [23], is to study the effect of adding some grain growth inhibitors such as Cr_3C_2 and TaC–NbC on the microstructure evolution and the main mechanical properties of SPSed WC–6Co cemented carbides.

2. Materials and methods

A WC–6Co powder mixture delivered by Kamb Import-Export, Poland (purity: 99.9%, APS: 100–200 nm), Cr_3C_2 powder (purity: 99.9%, APS: 6 μm) and TaC–NbC powder (purity: 99.9%, APS: 3 μm, ratio: 60:40) delivered by Inframat Advanced Materials, USA were used as the initial materials. The WC–6Co and Cr_3C_2, WC–6Co and TaC–NbC powders were mixed in a suspension of anhydrous acetone by means of ultrasonics for 5 min using a UP400S (Hielscher) homogenizer. The WC–6Co and prepared WC–6Co–$x$$Cr_3C_2$ and WC–6Co–xTaC–NbC (x = 1, 2, 3 wt%) powder mixtures were densified by SPS using an HP D 25-3 (FCT, Germany) furnace. For the WC–6Co powder mixture, the sintering temperature of 1400 °C was reached at the heating rates of 200 and 400 °C/min. The compacting pressure was kept constant at 50 and 60 MPa throughout the sintering process. The WC–6Co–$x$$Cr_3C_2$ and WC–6Co–xTaC–NbC (x = 1, 2, 3 wt%) powder mixtures were sintered at the temperature of 1400 °C which was reached at the heating rate of 400 °C/min. The compacting pressure was kept constant at 60 MPa throughout the sintering process. The vacuum in the sintering chamber was set at 0.05 mbar for all stages of the SPS processes. The holding time of 10 min was applied, after which the SPSed compacts were cooled to ambient temperature.

X-ray structural studies were performed using an Empyrean (PANalytical, Netherlands) diffractometer using Cu K_α radiation with an Ni filter, in the step scan mode. Microscopic observations and elemental microanalysis were performed by scanning electron microscopy using Vega 5135 (Tescan, Czech Republic), Inspect S and Quanta 250 FEG (FEI, Netherlands) microscopes equipped with EDS analysers. The densities of the consolidated materials were measured following the Archimedes' method. Vickers hardness measurements using an FV-700 (Future-Tech, Germany) hardness tester were carried out by applying a load of 294.2 N for 7 s. The fracture toughness (K_{1c}) was calculated based on the crack length measured from the corner of the indenter made by Vickers indentation using the following Eq. (1) [24],

$$K_{1c} = 0.15\sqrt{\frac{HV_{30}}{\Sigma l}} \tag{1}$$

where HV_{30} is the Vickers hardness measured under a load of 294.2 N and Σl is the total length of cracks initiated from the corners of the indenter.

3. Results and discussion

Density is one of the most important parameters of sintered materials characterization, and depends not only on the sintering conditions but also on the powder particle size and shape. Moreover, the particle size and shape influence the microstructure formation and mechanical strength of composites [25–27]. A decrease in the particle size results in an increase in the mechanical strength [4,28]. Fig. 1 shows micrographs of the initial powders. It can be seen that the WC–6Co powder mixture (Fig. 1a) consists of WC agglomerates irregular in shape and Co agglomerates spherical in shape. Probably the applied long mixing/milling time of the initial powders caused the WC particles to be covered by the Co particles and resulted in the formation of large agglomerates, whilst the WC particle size is in the range of 100–200 nm. Srivatsan et al. [28] in their investigations showed that using a WC particle size of 200 nm caused an increase in the density and microhardness of plasma pressure compacted (P^2C) WC ceramic with respect to larger particles. The Cr_3C_2 powder particles (Fig. 1b) were generally oval and slightly agglomerated in contrast to the TaC–NbC powder (Fig. 1c), which consists of significantly agglomerated particles nearly spherical in shape. The particle size of these powders is in the range of 3–6 μm, which is similar to data [29–32].

a)

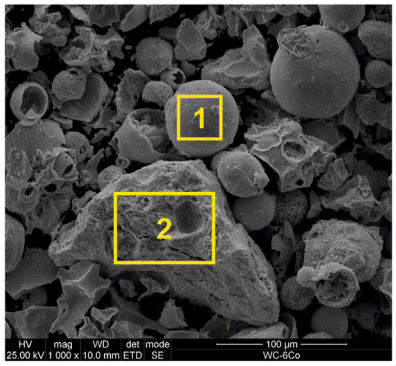

Element	# 1 [At%]	# 2 [At%]
W	51.55	49.56
C	38.72	41.39
Co	09.73	09.05

b)

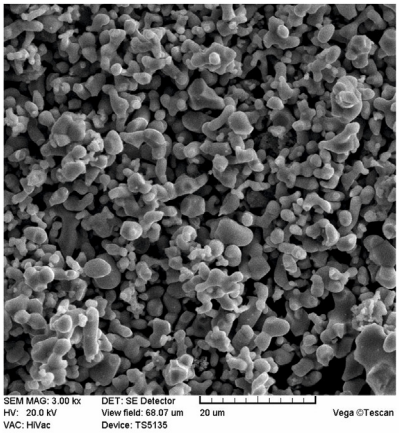

Element	[At%]
Cr	66.69
C	33.31

c)

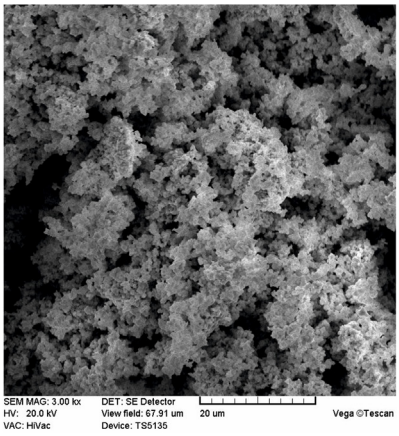

Element	[At%]
Ta	5.04
Nb	5.48
C	89.48

Fig. 1 – Second electron SEM micrographs and EDS analysis results of: (a) WC–6Co, (b) Cr_3C_2, (c) TaC–NbC initial powders, various magnifications.

Table 1 – Properties of spark plasma sintered tool materials.

Material	Effective density [g/cm^3]	Relative density [%]	Hardness [HV_{30}]	K_{1c} [MPa m$^{1/2}$]
WC–6Co 50/200	14.74	98.39	1775 ± 6	9.19 ± 0.30
WC–6Co 50/400	14.83	98.99	1773 ± 5	9.49 ± 0.34
WC–6Co 60/200	14.85	99.13	1704 ± 41	9.65 ± 0.61
WC–6Co 60/400	14.87	99.26	1712 ± 55	9.84 ± 0.49
WC–6Co–1Cr_3C_2	14.45	97.64	1808 ± 19	10.17 ± 0.27
WC–6Co–2Cr_3C_2	14.13	96.65	1791 ± 47	9.36 ± 0.31
WC–6Co–3Cr_3C_2	13.98	96.81	1689 ± 30	9.76 ± 0.22
WC–6Co–1TaC–NbC	14.57	97.72	1769 ± 32	9.69 ± 0.50
WC–6Co-2TaC–NbC	14.55	97.98	1787 ± 14	9.76 ± 0.22
WC–6Co–3TaC–NbC	14.52	98.24	1673 ± 37	9.72 ± 0.35

The changes in density with respect to compacting pressure and heating rate are listed in Table 1. All the obtained WC–6Co SPSed compacts are characterized by a relative density over 98.39%. The density increases with an increasing compacting pressure and heating rate. However, the results reveal that the influence of the heating rate plays a secondary role. The lowest relative density of 98.39% was exhibited by the WC–6Co SPSed at 50 MPa at 200 °C/min. Doubling the heating rate up to 400 °C/min caused an increase in the relative density by 0.60% (from 98.39 to 98.99%). It seems to be the effect of the greater amount of energy needed for more rapid heating of the powder, resulting in a higher current density and more intensive diffusion process intensifying the consolidation. This effect was described by authors [33] in detail. The WC–6Co cemented carbides SPSed at 60 MPa at 200 and 400 °C/min are characterized by relative densities of 99.13% and 99.26% respectively. It means that the heating rate does not effect on the densification process at a high compacting pressure at the near full density. The relative density increased by 0.13% at this case. Raising the compacting pressure from 50 to 60 MPa increased the relative density by 0.74 and 0.27% for the compacts SPSed at 200 and 400 °C/min respectively, which clearly shows the important role of compacting pressure in WC–Co materials SPS process. Additionally, one would note the obtained results are similar to those presented in paper [23] where the same WC–6Co powder mixture was SPSed at the same compacting pressure and heating rate at the lower sintering temperature (1200 °C). Only the compacts SPSed at 60 MPa had the density slightly lower, that revealed about the near full densification. Modifying the microstructure of WC–6Co cemented carbides by adding Cr_3C_2 and TaC–NbC grain growth inhibitors of various contents ranging between 1 and 3 wt% changed the density of the SPSed compacts. The main reason of an increase of the WC–6Co cemented carbides porosity with the additives is the higher viscosity of the locally occurring liquid Co phase containing Cr_3C_2, TaC and NbC particles and the lower capability to fill the pore space during sintering [20]. The same effect was described in our previous work [29] and work [30]. It is well-known that the average sintering temperature at SPS is far lower than that of conventional sintering due to the electrical spark discharges in the gaps between the powder particles (especially in the primary stage of sintering) that can generate a locally extremely high temperature on the surface of the powder particles [34] and a high-temperature spark plasma can be formed [35]. The relative density of the obtained cemented carbides decreases with increasing of Cr_3C_2 content and grows with increasing of TaC–NbC content. The density of the SPSed compacts with the Cr_3C_2 additive is lower than that of composite with the TaC–NbC additive because the theoretical density of Cr_3C_2 (6.68 g/cm^3) is significantly lower than TaC–NbC with a 60:40 ratio (10.35 g/cm^3).

The X-ray spectra of SPSed WC–6Co cemented carbides are presented in Fig. 2 and WC–6Co–xCr_3C_2, WC–6Co–xTaC–NbC (x = 1, 2, 3 wt%) spectra are shown in Fig. 3. The X-ray spectra exhibit peaks of hexagonal W_2C phase (ICDD 01-071-6323) and cubic η phases, Co_3W_3C (M_6C) (ICDD 00-006-0639), Co_6W_6C ($M_{12}C$) (ICDD 00-022-0597) besides the hexagonal WC phase (ICDD 01-089-2727). What is important, the Co phase is not visible in these spectra because X-ray structural study is not sensitive to Co [36]. The X-ray results of WC phase decarburization occurring at a lower compacting pressure are in agreement with the change in mechanical properties (rise in hardness and fall in fracture toughness as shown in Table 1). The possible mechanism of such microstructure formation process is the diffusion of carbon between the WC and Co phases at the spark areas during locally occurring sintering with the liquid phase. The similar mechanisms of WC–Co composites microstructure formation during liquid phase sintering were described by Eso and Fang [37,38]. They propose that formation of the cobalt gradient is the result of (1) carbon diffusion and migration of the liquid phase to attain an equilibrium phase composition as a function of the carbon content distribution, and (2) phase reactions between carbon and the Co phase. In our case, increasing the compacting pressure from 50 to 60 MPa results in diminution of the carbon diffusion processes. The possible explanation for this phenomenon based on some fundamentals of SPS [35,39–42] is that an increase in the compacting pressure and heating rate result in growth of the interparticle contact area and a decline of the current density at the particle–particle contacts. The result is diminishing of the Joule heating effects of the powder particles that leads to a smaller volume of Co liquid phase at the interparticle contacts at compacting pressure of 60 MPa. A

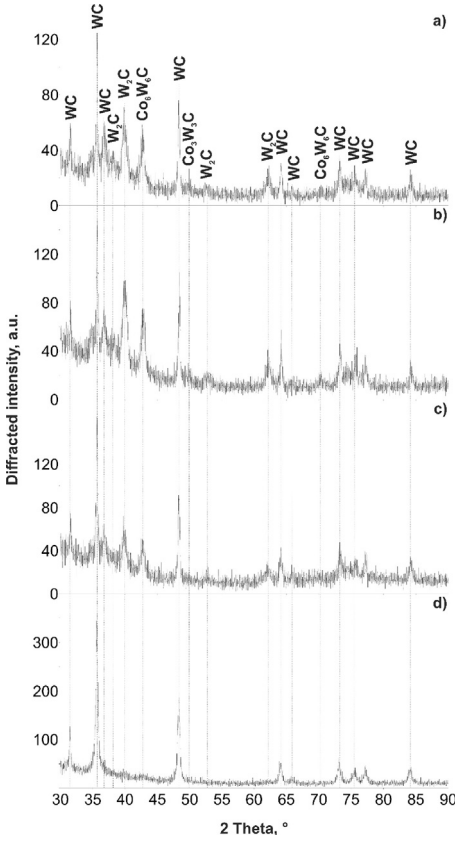

Fig. 2 – X-ray spectra of WC–6Co spark plasma sintered at compacting pressures and heating rates: (a) 50 MPa and 200 °C/min, (b) 50 MPa and 400 °C/min, (c) 60 MPa and 200°/min, and (d) 60 MPa and 400 °C/min.

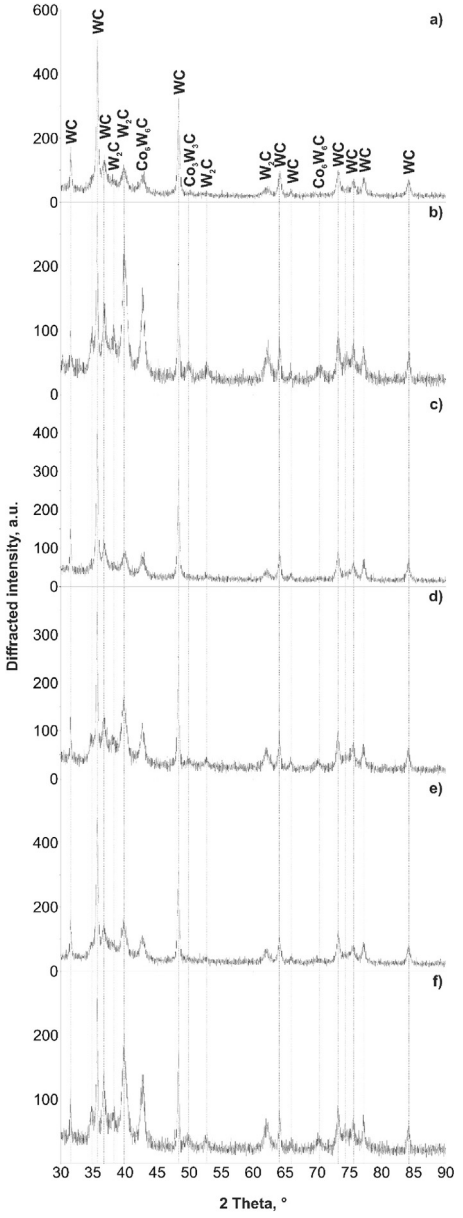

Fig. 3 – X-ray spectra of spark plasma sintered WC–6Co–$x$$Cr_3C_2$, where (a) x = 1, (b) x = 2, (c) x = 3 wt% and WC–6Co–xTaC–NbC, where (d) x = 1, (e) x = 2, and (f) x = 3 wt%.

decrease of the liquid phase volume results in a fall of the carbon diffusion rate between the WC phase and liquid Co phase and thus inhibits the formation of carbon deficient W_2C phase and η phases. Contrary, the contact area between neighboring powder particles during sintering at compacting pressure of 50 MPa is smaller than that of interparticle contacts created at the compacting pressure of 60 MPa, that results in a higher current density. It leads to increase of hot spots number and Joule overheating. An enhanced of the melting process leads to an increase of the carbon diffusion rate.

On the other hand, the X-ray spectra of the WC–6Co–$x$$Cr_3C_2$ and WC–6Co–xTaC–NbC (x = 1, 2, 3 wt%) cemented carbides show that the content of the secondary phases in these materials is higher than that of inhibitor-free WC–6Co compacts SPSed employing the same process parameters. The intensity of the peaks visible in the X-ray spectra is varied, that indicates about a different proportion of W_2C, Co_3W_3C and Co_6W_6C phases. The highest content of these phases is seen at the WC–6Co–2Cr_3C_2, WC–6Co–1TaC–NbC and WC–6Co–3TaC–NbC spectra.

The microstructures of the SPSed WC–6Co cemented carbides are presented in Fig. 4 and WC–6Co with grain growth inhibitors in Fig. 5. The elemental microanalysis showed that the bright contrast phase is the WC ceramic and the dark gray contrast phase is the Co binder. Moreover, the small black points (up to approx. 500 nm) nearly spherical in shape are the η phases. In the compacts SPSed at 200 °C/min at 50 MPa the number of these points is higher than in the compacts SPSed at 400 °C/min at 60 MPa, which confirms the results obtained by the X-ray studies, highlighting the fact that the presence of secondary phases decreases with an increasing compacting pressure and heating rate. Based on the microstructure of the WC6–Co cemented carbide SPSed at 400 °C/min at 60 MPa, the addition of Cr_3C_2 and TaC–NbC grain growth inhibitors affected the microstructure evolution in terms of more intensive formation of secondary phases. Furthermore, these phases appear in the form of agglomerates and are located at the WC particle boundaries (Fig. 5c and f).

The hardness and fracture toughness of SPSed cemented carbides are listed in Table 1. The WC–6Co cemented carbides SPSed at the lower compacting pressure of 50 MPa are characterized by a higher hardness (1775 ± 6 and 1773 ± 5 HV_{30}) and a lower fracture toughness (9.19 ± 0.30 and 9.49 ± 0.34 MPa $m^{1/2}$) than compacts SPSed at the higher compacting pressure of 60 MPa (1704 ± 41 HV_{30}, 9.65 MPa $m^{1/2}$ and 1712 ± 55 HV_{30}, 9.84 ± 0.49 MPa $m^{1/2}$). The same effect was observed in our previous study [23], where the lower sintering temperature was applied. Despite the fact that the density of compacts SPSed at 50 MPa is lower than that obtained at 60 MPa, the higher content of hard and brittle W_2C, Co_3W_3C and Co_6W_6C phases increased the hardness of these sintered compacts, especially when the heating rate was lower. Generally, the formation of these phases in WC–Co cemented carbides is undesirable since their presence lowers the fracture toughness [43,44]. The highest fracture toughness (9.84 ± 0.49 MPa $m^{1/2}$) was achieved for the compacts SPSed at 60 MPa and 400 °C/min. In this case the presence of these secondary phases was minimal.

The WC–6Co cemented carbides with the additions of Cr_3C_2 and TaC–NbC grain growth inhibitors (up to 2 wt%) are characterized by a higher hardness than the inhibitor-free WC–6Co cemented carbides. A further increase in the content of these additives diminishes the mechanical properties, probably due to the formation of large sized agglomerates, which are clearly visible in Fig. 5c (WC–6Co–3Cr_3C_2) and Fig. 5f (WC–6Co–3TaC–NbC). The hardness of these cemented carbides is the lowest (1689 ± 30 and 1673 ± 37 HV_{30} respectively). The hardness of the WC–6Co with 1 and 2 wt% additions of Cr_3C_2 (1808 ± 19 and 1791 ± 47 HV_{30}) is not significantly higher than that of composites with TaC–NbC additions (1769 ± 32 and 1787 ± 14 HV_{30}). The WC–6Co–1Cr_3C_2 cemented carbide

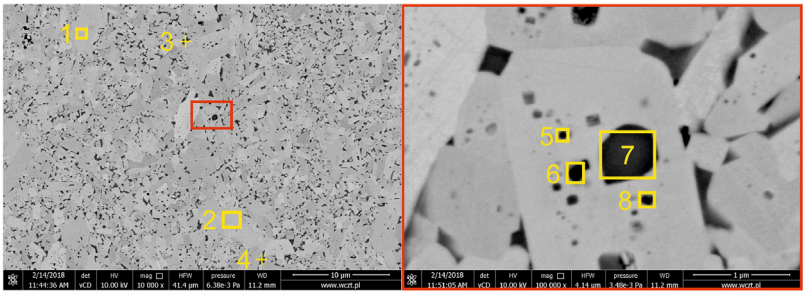

Element	# 1 [At%]	# 2 [At%]	# 3 [At%]	# 4 [At%]	# 5 [At%]	# 6 [At%]	# 7 [At%]	# 8 [At%]
W	40.64	40.79	38.68	41.85	39.32	41.20	41.78	41.48
C	57.38	58.20	51.17	48.83	56.07	46.15	39.11	52.45
Co	01.98	01.01	10.14	09.32	04.61	12.65	19.12	06.07

a)

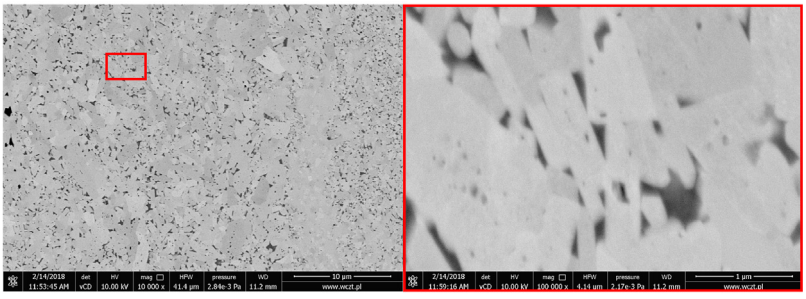

b)

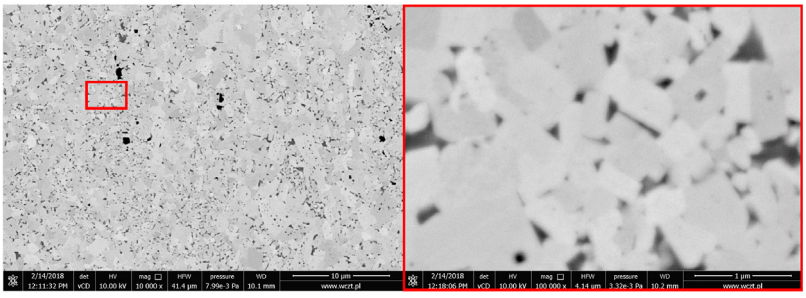

c)

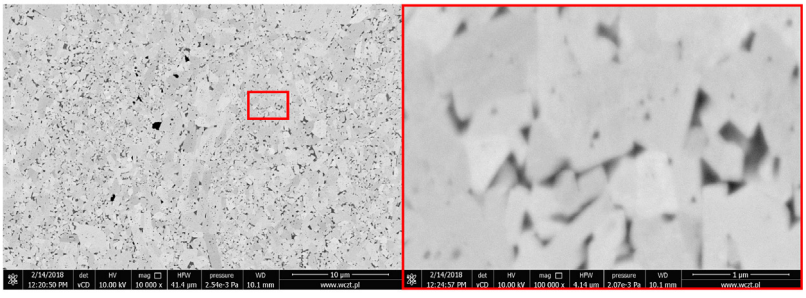

d)

Fig. 4 – Backscattered SEM micrographs of WC–6Co tool materials spark plasma sintered at: (a) 50 MPa and 200 °C/min, (b) 50 MPa and 400 °C/min, (c) 60 MPa and 200 °C/min, and (d) 60 MPa and 400 °C/min.

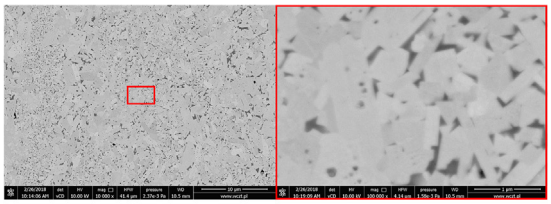

a)

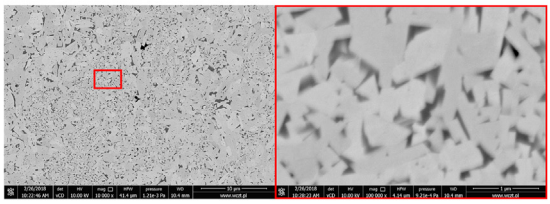

b)

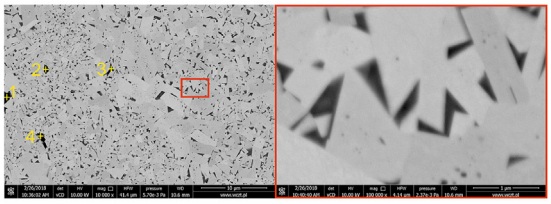

Element	# 1 [At%]	# 2 [At%]	# 3 [At%]	# 4 [At%]
Cr	81.98	83.55	80.91	80.45
C	18.02	16.45	19.09	19.55

c)

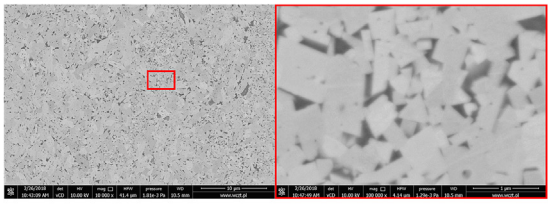

d)

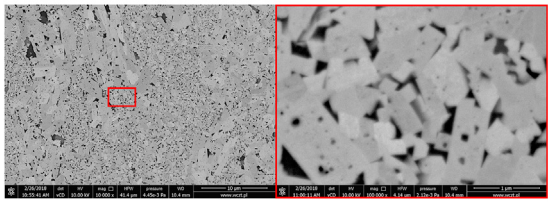

e)

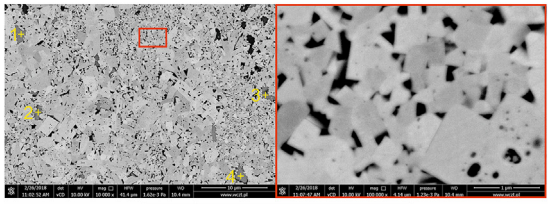

Element	# 1 [At%]	# 2 [At%]	# 3 [At%]	# 4 [At%]
Ta	21.03	18.59	22.68	22.82
Nb	26.28	28.63	24.77	25.10
C	52.68	52.78	52.55	52.08

f)

Fig. 5 – Backscattered SEM micrographs of spark plasma sintered WC–6Co–xCr_3C_2, where (a) x = 1, (b) x = 2, (c) x = 3 wt% and WC–6Co–xTaC–NbC, where (d) x = 1, (e) x = 2, and (f) x = 3 wt%.

has not only the highest hardness but also the highest fracture toughness of 10.17 ± 0.27 MPa $m^{1/2}$. Contrary, the fracture toughness of the WC–6Co–2TaC–NbC is lower (9.76 ± 0.22 MPa $m^{1/2}$) than that of WC–6Co–1Cr_3C_2 cemented carbide because the content of W_2C phase in the microstructure is slightly higher. In other cases where the content of the W_2C, Co_3W_3C and Co_6W_6C phases is higher, the fracture toughness ranges between 9.36 ± 0.31 and 9.76 ± 0.22 MPa $m^{1/2}$, which of course are acceptable values in view of the potential use of these materials for, e.g. cutting inserts (commercial H10S insert from the ISO K10 group fabricated by Baildonit, Poland having the composition of WC–4.5Co–4.5TaC–NbC has a hardness of 1650 HV_{30} and fracture toughness of 9.75 MPa $m^{1/2}$).

4. Conclusions

WC–Co, WC–Co–Cr_3C_2 and WC–Co–TaC–NbC cemented carbides were successfully fabricated by means of spark plasma sintering with varied process parameters such as the heating rate and compacting pressure in the case of WC–Co and varying weight contents of grain growth inhibitors in the case of WC–Co–Cr_3C_2 and WC–Co–TaC–NbC. The microstructure and mechanical properties of the WC–Co cemented carbides were investigated. The main conclusions are:

- during spark plasma sintering, decarburization of the WC phase occurred and W_2C, Co_3W_3C and Co_6W_6C secondary phases were formed,
- the relative density of WC–Co cemented carbides increases with an increasing compacting pressure and heating rate, however, the influence of the heating rate plays a secondary role,
- the relative density decreases with an increasing content of Cr_3C_2 and increases with an increasing content of TaC–NbC grain growth inhibitors, whereas in the SPSed compacts with the Cr_3C_2 additive the relative density is lower than using the TaC–NbC additive,
- the WC–6Co cemented carbides SPSed at the lower compacting pressure of 50 MPa are characterized by a higher hardness (1773 ± 5 and 1775 ± 6 HV_{30}) than the compacts SPSed at the higher compacting pressure of 60 MPa (1704 ± 41 and 1712 ± 55 HV_{30}). The reason is the higher content of hard W_2C, Co_3W_3C and Co_6W_6C phases formed in WC–Co SPSed at 50 MPa,
- the synthesized secondary phases, widely recognized as undesirable in WC–Co cemented carbides, in these cases do not significantly reduce the investigated mechanical properties, especially fracture toughness,
- the best ratio of hardness and fracture toughness was obtained by WC–6Co–1Cr_3C_2 whose hardness is 1808 ± 19 HV_{30} and fracture toughness is 10.17 ± 0.27 MPa $m^{1/2}$.

Conflict of interest

None declared.

Ethical statement

Authors state that the research was conducted according to ethical standards.

Funding body

Ministry of Science and Higher Education Republic of Poland.

Acknowledgements

The study was carried out within the statutory work of the Metal Forming Institute in Poznan BS 901 51 entitled ''*Manufacturing composite materials on the matrix of cobalt and its alloys for applications in modern economy sectors by the spark plasma sintering method (SPS)*''.

The authors would like to thank Prof. Volf Leshchynsky for his helpful advices and comments.

REFERENCES

[1] A.L. Armstead, B. Li, Nanotoxicity: emerging concerns regarding nanomaterial safety and occupational hard metal (WC–Co) nanoparticle exposure, Int. J. Nanomed. 11 (2016) 6421–6433.
[2] D. Lison, R. Lauwerys, The interaction of cobalt metal with different carbides and other mineral particles on mouse peritoneal macrophages, Toxicol. Vitro 9 (1995) 341–347.
[3] W. Liu, X. Song, K. Wang, J. Zhang, G. Zhang, X. Liu, A novel rapid route for synthesizing WC–Co bulk by in situ reactions in spark plasma sintering, Mater. Sci. Eng. A 499 (2009) 476–481.
[4] W. Liu, X. Song, J. Zhang, F. Yin, G. Zhang, A novel route to prepare ultrafine-grained WC–Co cemented carbides, J. Alloys Compd. 458 (2008) 366–371.
[5] R.M. Raihanuzzaman, T.S. Jeong, R. Ghomashchi, Z. Xie, S.-J. Hong, Characterization of short-duration high-energy ball milled WC–Co powders and subsequent consolidations, J. Alloys Compd. 615 (2014) S564–S568.
[6] H.-C. Kim, I.-J. Shon, J.-K. Yoon, J.-M. Doh, Consolidation of ultra fine WC and WC–Co hard materials by pulsed current activated sintering and its mechanical properties, Int. J. Refractory Metals Hard Mater. 25 (2007) 46–52.
[7] K.T. Akihiro Nino, Shigeaki Sugiyama, Hitoshi Taimatsu, Effects of carbon addition on microstructures and mechanical properties of binderless tungsten carbide, Mater. Trans. 53 (2012) 1475–1480.
[8] F.A. Deorsola, D. Vallauri, G.A. Ortigoza Villalba, B.D. Benedetti, Densification of ultrafine WC–12Co cermets by pressure assisted fast electric sintering, Int. J. Refract. Metals Hard Mater. 28 (2010) 254–259.
[9] R. Bao, J.-h. Yi, Y.-d. Peng, H.-z. Zhang, A.-k. Li, Decarburization and improvement of ultra fine straight WC–8Co sintered via microwave sintering, Trans. Nonferrous Metals Soc. China 22 (2012) 853–857.
[10] P. Arató, L. Bartha, R. Porat, S. Berger, A. Rosen, Solid or liquid phase sintering of nanocrystalline WC/Co hardmetals, Nanostructured Mater. 10 (1998) 245–255.
[11] C. Jia, L. Sun, H. Tang, X. Qu, Hot pressing of nanometer WC–Co powder, Int. J. Refract. Metals Hard Mater. 25 (2007) 53–56.
[12] C. Wei, X. Song, S. Zhao, L. Zhang, W. Liu, In-situ synthesis of WC–Co composite powder and densification by sinter-HIP, Int. J. Refract. Metals Hard Mater. 28 (2010) 567–571.
[13] R. Bao, J. Yi, Effect of sintering atmosphere on microwave prepared WC–8 wt.%Co cemented carbide, Int. J. Refract. Metals Hard Mater. 41 (2013) 315–321.
[14] H.-C. Kim, D.-Y. Oh, I.-J. Shon, Sintering of nanophase WC–15vol.%Co hard metals by rapid sintering process, Int. J. Refract. Metals Hard Mater. 22 (2004) 197–203.
[15] H.-C. Kim, D.-Y. Oh, J. Guojian, I.-J. Shon, Synthesis of WC and dense WC–5vol.% Co hard materials by high-frequency induction heated combustion, Mater. Sci. Eng. A 368 (2004) 10–17.
[16] R.M. Raihanuzzaman, M. Rosinski, Z. Xie, R. Ghomashchi, Microstructure and mechanical properties and of pulse plasma compacted WC–Co, Int. J. Refract. Metals Hard Mater. 60 (2016) 58–67.
[17] M.R. Rumman, Z. Xie, S.-J. Hong, R. Ghomashchi, Effect of spark plasma sintering pressure on mechanical properties of WC–7.5wt% Nano Co, Mater. Design 68 (2015) 221–227.
[18] S. Zhao, X. Song, C. Wei, L. Zhang, X. Liu, J. Zhang, Effects of WC particle size on densification and properties of spark plasma sintered WC–Co cermet, Int. J. Refract. Metals Hard Mater. 27 (2009) 1014–1018.
[19] L. Espinosa-Fernández, A. Borrell, M.D. Salvador, C.F. Gutierrez-Gonzalez, Sliding wear behavior of WC–Co–Cr_3C_2–VC composites fabricated by conventional and non-conventional techniques, Wear 307 (2013) 60–67.
[20] M. Mahmoodan, H. Aliakbarzadeh, R. Gholamipour, Sintering of WC–10%Co nano powders containing TaC and VC grain growth inhibitors, Trans. Nonferrous Metals Soc. China 21 (2011) 1080–1084.
[21] R. van der Merwe, N. Sacks, Effect of TaC and TiC on the friction and dry sliding wear of WC–6 wt.% Co cemented carbides against steel counterfaces, Int. J. Refract. Metals Hard Mater. 41 (2013) 94–102.
[22] R.M. Genga, G. Akdogan, J.E. Westraadt, L.A. Cornish, Microstructure and material properties of PECS manufactured WC–NbC–CO and WC–TiC–Ni cemented carbides, Int. J. Refract. Metals Hard Mater. 49 (2015) 240–248.
[23] D. Garbiec, P. Siwak, Microstructure and properties of spark plasma sintered WC–6Co cemented carbides, Metal Forming 28 (2017) 123–132.
[24] W.D. Schubert, H. Neumeister, G. Kinger, B. Lux, Hardness to toughness relationship of fine-grained WC–Co hardmetals, Int. J. Refract. Metals Hard Mater. 16 (1998) 133–142.
[25] G.S. Upadhyaya, Cemented Tungsten Carbides: Production, Properties, and Testing, William Andrew Publishing, Westwood, NJ, 1998.
[26] R.S. Parihar, S. Gangi Setti, R.K. Sahu, Preliminary investigation on development of functionally graded cemented tungsten carbide with solid lubricant via ball milling and spark plasma sintering, J. Compost. Mater. 52 (2018) 1363–1377.
[27] A. Simchi, F. Petzoldt, Cosintering of powder injection molding parts made from ultrafine WC–Co and 316L stainless steel powders for fabrication of novel composite structures, Metall. Mater. Trans. A 41 (2009) 233.
[28] T.S. Srivatsan, R. Woods, M. Petraroli, T.S. Sudarshan, An investigation of the influence of powder particle size on microstructure and hardness of bulk samples of tungsten carbide, Powder Technol. 122 (2002) 54–60.
[29] P. Siwak, D. Garbiec, Microstructure and mechanical properties of WC–Co, WC–Co–Cr_3C_2 and WC–Co–TaC cermets fabricated by spark plasma sintering, Trans. Nonferrous Metals Soc. China 26 (2016) 2641–2646.

[30] L. Sun, T.e. Yang, C. Jia, J. Xiong, VC, Cr_3C_2 doped ultrafine WC–Co cemented carbides prepared by spark plasma sintering, Int. J. Refract. Metals Hard Mater. 29 (2011) 147–152.
[31] L. Sun, C. Jia, R. Cao, C. Lin, Effects of Cr_3C_2 additions on the densification, grain growth and properties of ultrafine WC–11Co composites by spark plasma sintering, Int. J. Refract. Metals Hard Mater. 26 (2008) 357–361.
[32] D.H. Xiao, Y.H. He, M. Song, N. Lin, R.F. Zhang, Y2O3- and NbC-doped ultrafine WC–10Co alloys by low pressure sintering, Int. J. Refract. Metals Hard Mater. 28 (2010) 407–411.
[33] D. Garbiec, P. Siwak, J. Jakubowicz, The effect of heating rate and sintering time on properties of WC–6Co nanocrystalline composites produced by spark plasma sintering, Compos. Theory Practice 15 (2015) 48–53.
[34] X. Wang, Y. Xie, H. Guo, O. Van der Biest, J. Vleugels, Sintering of WC–Co powder with nanocrystalline WC by spark plasma sintering, Rare Metals 25 (2006) 246–252.
[35] Z.-H. Zhang, Z.-F. Liu, J.-F. Lu, X.-B. Shen, F.-C. Wang, Y.-D. Wang, The sintering mechanism in spark plasma sintering – proof of the occurrence of spark discharge, Scr. Mater. 81 (2014) 56–59.
[36] R. Jenkins, R.L. Snyder, Introduction to X-ray Powder Diffractometry, Wiley Online Library, 1996.
[37] O. Eso, Z. Fang, A. Griffo, Liquid phase sintering of functionally graded WC–Co composites, Int. J. Refract. Metals Hard Mater. 23 (2005) 233–241.
[38] O. Eso, Z.Z. Fang, A. Griffo, Kinetics of cobalt gradient formation during the liquid phase sintering of functionally graded WC–Co, Int. J. Refract. Metals Hard Mater. 25 (2007) 286–292.
[39] X. Song, X. Liu, J. Zhang, Mechanism of conductive powder microstructure evolution in the process of SPS, Sci. China Ser. E Eng. Mater. Sci. 48 (2005) 258–269.
[40] C. Collard, Z. Trzaska, L. Durand, J.-M. Chaix, J.-P. Monchoux, Theoretical and experimental investigations of local overheating at particle contacts in spark plasma sintering, Powder Technol. 321 (2017) 458–470.
[41] C. Manière, A. Pavia, L. Durand, G. Chevallier, K. Afanga, C. Estournès, Finite-element modeling of the electro-thermal contacts in the spark plasma sintering process, J. Eur. Ceram. Soc. 36 (2016) 741–748.
[42] O. Guillon, J. Gonzalez-Julian, B. Dargatz, T. Kessel, G. Schierning, J. Räthel, M. Herrmann, Field-assisted sintering technology/spark plasma sintering: mechanisms, materials, and technology developments, Adv. Eng. Mater. 16 (2014) 830–849.
[43] F.C.M.A. Formisano, A. Caraviello, L. Carrino, M. Durante, A. Langella, Influence of eta-phase on wear behavior of WC–Co carbides, Adv. Tribol. 2016 (2016) 6.
[44] M. Sakaki, M.S. Bafghi, J. Vahdati Khaki, Q. Zhang, F. Saito, Conversion of W2C to WC phase during mechano-chemical synthesis of nano-size WC–Al_2O_3 powder using WO_3-2Al–(1 + x) C mixtures, Int. J. Refract. Metals Hard Mater. 36 (2013) 116–121.